Bioorganic & Medicinal Chemistry Letters 24 (2014) 4132–4140

Contents lists available at ScienceDirect

Bioorganic & Medicinal Chemistry Letters

journal homepage: www.elsevier.com/locate/bmcl

Kinase domain inhibition of leucine rich repeat kinase 2 (LRRK2) using a [1,2,4]triazolo[4,3-*b*]pyridazine scaffold

Paul Galatsis [a,*], Jaclyn L. Henderson [a], Bethany L. Kormos [a], Seungil Han [b], Ravi G. Kurumbail [b], Travis T. Wager [a], Patrick R. Verhoest [a], G. Stephen Noell [c], Yi Chen [d], Elie Needle [d], Zdenek Berger [d], Stefanus J. Steyn [e], Christopher Houle [f], Warren D. Hirst [d]

[a] *Worldwide Medicinal Chemistry, Pfizer Worldwide R&D, 610 Main St., Cambridge, MA 02139, United States*
[b] *Worldwide Medicinal Chemistry, Pfizer Worldwide R&D, Eastern Point Rd., Groton, CT 06340, United States*
[c] *Primary Pharmacology Group, Pfizer Worldwide R&D, Eastern Point Rd., Groton, CT 06340, United States*
[d] *Neuroscience Research Unit, Pfizer Worldwide R&D, 610 Main St., Cambridge, MA 02139, United States*
[e] *Pharmacokinetics, Dynamics, and Metabolism, Pfizer Worldwide R&D, 610 Main St., Cambridge, MA 02139, United States*
[f] *Drug Safety R&D, Pfizer Worldwide R&D, Eastern Point Rd., Groton, CT 06340, United States*

ARTICLE INFO

Article history:
Received 16 July 2014
Accepted 18 July 2014
Available online 30 July 2014

Keywords:
Leucine rich repeat kinase 2
LRRK2
Kinase inhibitors
Triazolopyridazine

ABSTRACT

Leucine rich repeat kinase 2 (LRRK2) has been genetically linked to Parkinson's disease (PD). The most common mutant, G2019S, increases kinase activity, thus LRRK2 kinase inhibitors are potentially useful in the treatment of PD. We herein disclose the structure, potential ligand–protein binding interactions, and pharmacological profiling of potent and highly selective kinase inhibitors based on a triazolopyridazine chemical scaffold.

Parkinson's disease (PD) is the most common movement disorder and the second most common neurodegenerative disorder after Alzheimer's disease (AD).[1] Significant excitement has been generated by recent genome-wide association studies (GWAS) that linked the PARK8 mutation, encoding the leucine rich repeat kinase 2 (LRRK2) protein, to PD.[2] LRRK2 is a very large protein (2527 amino acids; 286 kDa MW) comprised of multiple domains (Fig. 1).[3] The most common LRRK2 mutation is G2019S (GS) which is in the activation loop (DFG motif-DYG in LRRK2) of the kinase domain.[4] This mutation has been reported to increase the kinase activity of LRRK2, thus the identification of potent, selective, brain penetrant kinase inhibitors could dampen this hyperactivity and be of value in the treatment of PD.[5]

LRRK2 linkage to PD is a very recent discovery and a significant amount of LRRK2 biology relating to PD has yet to be elucidated.[6] One key gap is our lack of understanding of the exact role of LRRK2 in PD. In an effort to gain insight into its PD role, various groups have explored LRRK2 biology with re-purposed kinase inhibitors.[7] Other groups sought to identify novel chemical tools with a goal of improving kinase specificity.[8] Utilization of modestly selective tool compounds to probe the biology of LRRK2 can be problematic in that it generates data that is difficult to interpret, as one needs to de-convolute on-target from off-target pharmacology.[9] Although the discovery of potent and selective LRRK2 kinase inhibitors may be challenging and require significant investment of resources, they should allow for a robust understanding of the biological consequences of LRRK2 inhibition. Thus, in our efforts to develop LRRK2 kinase inhibitors, potency, selectivity, in vivo efficacy and brain penetration were all tracked in an effort to generate

Abbreviations: AD, Alzheimer's disease; ANK, ankyrin repeat domain; ARM, armadillo repeat domain; AUC, area under the curve; BA, brain availability; BBB, blood brain barrier; BCRP, breast cancer related protein; BI, brain impairment; CSD, Cambridge Structural Database; CNS, central nervous system; COR, C-terminal of ROC domain; ER, efflux ratio; GS, LRRK2 G2019S mutation; GWAS, genome-wide association studies; HLM, human liver microsome; HTS, high throughput screening; KO, knockout; $K_{p,uu}$, unbound brain to unbound plasma concentration ratio; KSS, kinase selectivity screening; LE, ligand efficiency; LipE, lipophilic ligand efficiency; LRR, leucine rich repeat domain; LRRK2, leucine rich repeat kinase 2; MDR1, multi-drug resistance protein 1 (human *P*-gp); MPO, multi-parameter optimization; PD, Parkinson's disease; PDB, protein data bank; PK/PD, pharmacokinetic/pharmacodynamic; ROC, ras of complex domain; SAR, structure activity relationship; WCA, whole cell assay based on pS935 readout; WD40, WD40 repeat domain; WT, wild type.

* Corresponding author. Tel.: +1 617 395 0709.
E-mail address: paul.galatsis@pfizer.com (P. Galatsis).

http://dx.doi.org/10.1016/j.bmcl.2014.07.052
0960-894X/

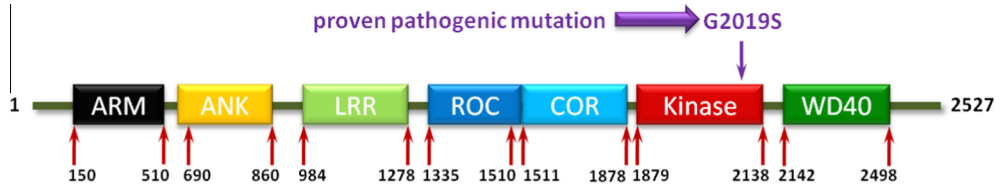

Figure 1. Multi-domain structure of LRRK2.

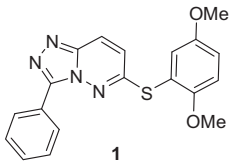

50 μM ATP LRRK2 (WT) IC_{50} = 40 nM
LE = 0.39; LipE = 3.6; CNS MPO = 4.82
1 mM ATP LRRK2 (WT) IC_{50} = 173 nM
1 mM ATP LRRK2 (GS) IC_{50} = 82 nM
HLM $CL_{IA,S}$ = 159 mL/min/kg
P_{app} AB = 12 x 10^{-6} cm/sec
MDR1 ER (BA/AB) = 1.77
KSS = 0/39 hits at 1 μM

Figure 2. Data summary of HTS hit **1**.

the most efficient inhibitors for potential treatment of PD. In this Letter, we disclose our optimization of a triazolopyridazine scaffold targeting the LRRK2 kinase domain.

A high throughput screen (HTS) of about 750,000 compounds allowed us to identify multiple scaffolds including triazolopyridazine **1** as a potent inhibitor of LRRK2, which bears high similarity to a hit recently described by scientists at Elan (Fig. 2).[8i] It exhibited double-digit nM potency in a LANTHA screen assay at the ATP K_M (50 μM) of LRRK2.[10] Shifting the ATP concentration to one more physiologically relevant (1 mM) resulted in a modest rightward shift in potency for both the WT and the GS mutation.[10] Along with its desirable in vitro potency, **1** exhibited physicochemical properties consistent with CNS drug space (e.g. high LE, LipE and good CNS MPO score).[11] This observation was buttressed by in vitro data showing excellent kinase selectivity,[12] high passive permeability, and a lack of *P*-gp transporter-mediated membrane asymmetry (good potential for brain availability). The HLM clearance was found to be high, as one might predict for a compound susceptible to an *O*-demethylation metabolic clearance pathway.

As part of our hit-to-lead approach, strict adherence to designing compounds with an eye to physicochemical properties was followed. Given that treating PD would involve a long-term, chronic regimen, minimizing daily dose and maximizing the safety profile were critical attributes that could be readily achieved, at the design stage, using this strategy. The CNS MPO score was a relatively straightforward yardstick to monitor our ability to align drug-like properties and all compounds presented in this Letter met or exceeded the cut-off for CNS drug-like space.[11c] In examining the sources of potential diversity within the di-substituted triazolopyridazine scaffold, 4 points of diversity were readily apparent; the 2 substituent moieties (at C_3 and C_6), the S-linker atom, and the hinge interaction core itself.

Our SAR optimization began with the C_3 substituent. Table 1 provides a summary of some of the compounds prepared in the evaluation of this position. While small alkyls (**7**), saturated hetero-cycles (**8**–**9**), and 6-membered ring heteroaromatics (**2**–**6**) showed varying degrees of potency, the 5-membered ring heteroaromatics (**11**–**16**) proved to be optimal for this diversity vector. In particular, methyl-pyrazole **15** became an obvious standout. Not only does this compound have improved potency (and LipE) but it also is the only compound that significantly reduced clearance whilst maintaining potency. Adding a methylene spacer to this moiety (**10**) resulted in a dramatic loss in potency. While not formally presented in the tables, G2019S IC_{50} values were determined and found to be roughly equipotent with the wt isoform (within ±3×). For all compounds tested in this series, we found a 5–10× rightward shift in potency in going from the cell free to whole cell assays[10] despite the good potency at cellularly relevant ATP concentrations and excellent passive permeability.

While our hit-to-lead efforts were ongoing, we were very interested in better understanding the potential binding interactions of these compounds. In the absence of LRRK2 crystallographic information, we employed a surrogate crystallography approach based on kinase similarity and cross-over of compound activity. Though LRRK2 only has ~30% residue identity and ~50% similarity in the overall kinase domain to its closest neighbors, the residues in its ATP-binding site pocket have greater similarity to a number of other kinases. For instance, tyrosine kinase 2 (Tyk2) ATP-binding site residues are 74% similar to those in LRRK2. In addition, there was some cross-over activity of this series of triazolopyridazine compounds with the JAK family of kinases (vide infra), suggesting Tyk2 is a reasonable surrogate crystallographic system for LRRK2.

With crystals of Tyk2 readily available from a previous project, we pursued soaking studies of **15** with Tyk2 to see if it could act as a model system and provide some insight into the potential binding interactions. Figure 3 shows the X-ray crystal structure of **15** in Tyk2 (PDB ID: 4PY1) highlighting several protein-ligand interactions. Compounds of this scaffold appear to make a single point interaction with kinase hinge via the C_1 *N*-atom of the triazole moiety, with the Me-pyrrazole occupying the ribose pocket (towards solvent) and not a position adjacent to gatekeeper, in contrast to a binding mode previously suggested for this chemotype.[8i]

Having identified optimal C_3 substituents, we next focused attention on the C_6-S substituent as it was a potential metabolic soft spot and safety liability (potential for quinone formation). Table 2 provides a sampling of substituents explored at this position. Compounds **17** and **18** provided evidence that the two methoxy groups of the phenyl ring were having a synergistic effect, in that, independently they provided weak potency to the scaffold but together, as in **1**, resulted in a dramatic increase in kinase inhibition. This is somewhat in contrast to the SAR reported by Elan, whereby they demonstrated LRRK2 potency with solely a *meta* substituted aryl at this position.[8i] The binding pose (Fig. 3) allows one to speculate if an interaction of the two methoxys with the *P*-loop and floor of the ATP site is required for good potency (observed with tofacitinib). This bioactive conformation could be favored by the *ortho*-OMe twisting the aryl ring orthogonal to the plane of the triazolopyridazine core. In support of this hypothesis, the *ortho*-OMe was found to be required, whereas, small substituents could be tolerated at the *meta*-position, for example, **19** and **20**. While **20** maintained good predicted brain availability, this change did increase clearance compared to **15**. Conversely, **19** showed a modest decrease in clearance but now had the potential for *P*-gp efflux susceptibility. Clearance could be greatly improved as **23** demonstrated, by modulating the potential phenyl metabolic soft spots, but could not be coupled with potency.

We were concerned the *S*-linker may be a metabolic liability and explored options for its replacement. While all of the compounds examined were predicted to be in good CNS space (MPO > 4), all linker replacements examined (ether **24**, amino **25**,

Table 1
SAR data for substitution at C_3 of [1,2,4]triazolo[4,3-*b*]pyridazine

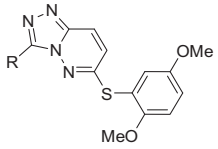

Compd	R	LRRK2 IC_{50}[a] (nM)	LE/LipE[b]	LRRK2 WC IC_{50} (nM)[c]	HLM[d]	P_{app}[e]	*P*-gp[f]
1		173	0.36/3.10	1380	159	12	1.77
2		496	0.33/3.84	1310	104	20	1.47
3		242	0.35/4.36	736	86	21	1.27
4		349	0.34/4.21	nt	77	26	1.25
5		880	0.32/4.58	nt	nt	nt	nt
6	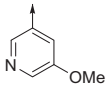	66	0.35/4.51	440	137	17	1.77
7		2290	0.33/3.36	nt	146	17	0.70
8		2489	0.31/4.32	nt	28	32	1.51
9		12,600	0.26/3.49	nt	nt	7.4	4.46
10		32,000	0.23/2.97	nt	nt	nt	nt
11		804	0.33/4.09	4330	30	30	1.16
12		91	0.38/4.38	722	195	20	1.66
13		95	0.38/4.76	660	71	26	1.65
14		224	0.35/4.57	2760	116	19	2.17
15		64	0.38/5.32	387	42	34	2.22
16		323	0.33/4.65	1260	106	16	1.80

[a] Geometric mean of $n \geqslant 2$ for wild-type LRRK2 at 1 mM ATP.
[b] Calculated from 1 mM ATP IC_{50} using *c*log*P* values.
[c] Geometric mean of $n \geqslant 2$ for whole cell pS935 determinations in wild-type LRRK2.
[d] Human liver microsomal clearance (mL/min/kg).
[e] Passive permeability (AB $\times 10^{-6}$ cm/s).
[f] MDR1 Efflux Ratio (BA/AB). nt = not tested.

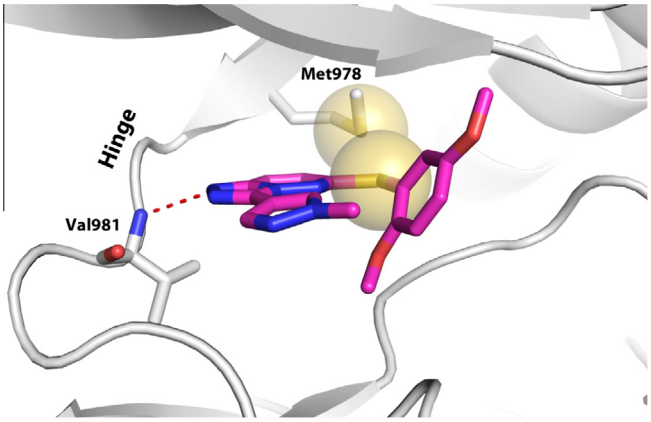

Figure 3. Crystal structure of Tyk2 in complex with **15** (4PY1).

methylene **27**, hydroxymethyl **28**, keto **29**, difluoromethyl **30**, and NMe **31**) did not show any improvement upon the *S*-linker (Table 3). It has been proposed, based on homology modeling, that the thioether dihedral (~90°) provides the requisite trajectory for this substituent compared to O, NH, or CH_2 linkers (dihedral >90°).[8i] Though we agree that the dihedral angle is important for interactions of the phenyl substituents with the pocket, we also believe the C–X–C angle (X = S, O, NH or CH_2) is important in obtaining optimal interactions with the Gly-rich loop and the rest of the binding pocket. Based on an analysis of structures in the Cambridge Structural Database (CSD)[13] using Mogul[14], the average aromatic C–S–aromatic C angle is ~103°, whereas when O, NH or CH_2 are substituted for S, the average angles are 120°, 128° and 114°, respectively. In addition, the indicated binding pose (Fig. 3) revealed a favorable S-S non-bonded interaction between the ligand and the Met[978] gatekeeper, which is conserved in LRRK2. The S-linker alternatives could be generating steric clashes with the gatekeeper Met.

The final feature of this scaffold subjected to SAR analysis was the core framework and the effect this may have on hinge binding (Table 4). Adding methyl substituents (as in compounds **32** and **33**) resulted in a dramatic loss of potency. Consistent with the binding pose (Fig. 3), Me or larger substituents at C_7 would cause a clash with the Met[1947] gatekeeper residue and substituents at C8 would severely clash with the Glu[1948] backbone carbonyl at the hinge (LRRK2 numbering).

Additional support for the bioactive conformation depicted in Figure 3 can be inferred from **34**. Substituting the pyridazine *N*-atom for a *C*-atom resulted in a significant decrease in potency

Table 2
SAR data for substitution at C_6-S of [1,2,4]triazolo[4,3-*b*]pyridazine

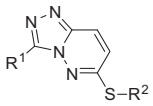

Compd	R^1	R^2	LRRK2 IC_{50}[a] (nM)	LE/LipE[b]	LRRK2 WC IC_{50}[c] (nM)	HLM[d]	P_{app}[e]	*P*-gp[f]
17		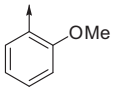	1070[g]	na	nt	164	7.3	1.51
18		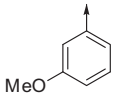	2110[g]	na	nt	189	3.8	1.72
19	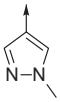	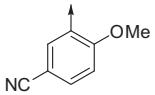	64	0.38/5.65	2070	28	19	3.87
20	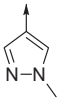	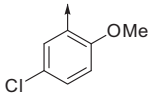	78	0.39/4.47	245	113	20	1.97
21	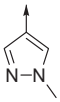	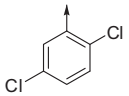	373	0.37/2.73	1800	72	10	1.60
22	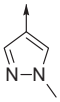	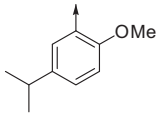	1350	0.30/2.66	nt	221	15	1.76
23	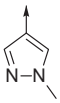	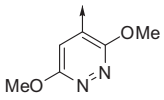	12,635	0.26/4.43	nt	<8	21	1.50

[a] Geometric mean of $n \geqslant 2$ for wild-type LRRK2 at 1 mM ATP.
[b] Calculated from 1 mM ATP IC_{50} using *c*log*P* values.
[c] geometric mean of $n \geqslant 2$ for whole cell pS935 determinations in wild-type LRRK2.
[d] human liver microsomal clearance (mL/min/kg).
[e] passive permeability (AB × 10^{-6} cm/s).
[f] MDR1 Efflux Ratio (BA/AB). nt = not tested.
[g] geometric mean of $n > 2$ for wild-type LRRK2 at K_M ATP.

Table 3
Linker-atom substitution of [1,2,4]triazolo[4,3-*b*]pyridazine

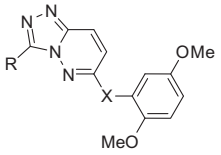

Compd	R	X	LRRK2 IC_{50}[a] (nM)	LE/LipE[b]	LRRK2 WC IC_{50}[c] (nM)	HLM[d]	P_{app}[e]	*P*-gp[f]
24		–O–	236	0.35/3.35	1740	168	15	1.26
25		–NH–	22,265[g]	na	nt	250	2.47	2.78
26	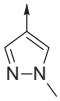	–O–	549	0.33/4.78	nt	nt	nt	nt
27	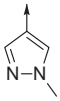	–CH_2–	6202	0.27/3.41	nt	18	19	1.59
28	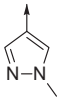	–CHOH–	9124	0.25/5.00	nt	<8	14	7.14
29	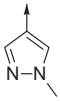	–CO–	1211	0.30/4.65	nt	60	16	2.02
30	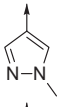	–CF_2–	763	0.30/4.62	nt	28	22	1.46
31	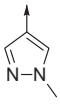	–NMe–	21,858	0.24/2.65	nt	13	14	1.58

[a] Geometric mean of $n \geqslant 2$ for wild-type LRRK2 at 1 mM ATP.
[b] Calculated from 1 mM ATP IC_{50} using *c*log*P* values.
[c] Geometric mean of $n \geqslant 2$ for whole cell pS935 determinations in wild-type LRRK2.
[d] Human liver microsomal clearance (mL/min/kg).
[e] Passive permeability ($AB \times 10^{-6}$ cm/s).
[f] MDR1 Efflux Ratio (BA/AB). nt = not tested.
[g] geometric mean of $n > 2$ for wild-type LRRK2 at K_M ATP.

relative to **15**. This could be attributed to the greater rotational flexibility of the C_6 substituent provided by the loss of a key non-bonding electron-electron repulsion present in **15**.

Modifying the scaffold core by manipulating the *N*-atom substitution pattern resulted in mixed results. Most of the changes gave rise to a loss in potency relative to **1**, however, **35** and **36**, the imidazo-pyridazine and pyrrazolopyrimidine cores, respectively, generated analogs that were equipotent to **15**. While these analogs maintained the predicted good brain availability (P_{app} and *P*-gp data), **35** and **36** did not provide any improvement in HLM clearance. Whereas, **15** did not exhibit significant activity in our internal KSS panel (i.e., >50 % inhibition at 1 μM), both **35** and **36** exhibited a 9/39 hit rate. While the overlap of these nine kinase hits for the compounds was not identical, the dramatic change in promiscuity was not anticipated. The binding pose (Fig. 3) indicated the N_2-atom points towards the backbone carbonyl of Ala^{1950}, which, due to its small side chain, may be more flexible to accommodate a water-mediated H-bond to this *N*-atom (observed in crystallographic data). The C–H at C_2 of **35** and **36** will likely form a non-traditional H-bond to the backbone carbonyl of Ala^{1950}, as well as kinases that have a larger amino acid side chain at that position, thus giving rise to the loss of selectivity.

Having identified **15** as a potent LRRK2 inhibitor with high kinome selectivity from internal profiling (0/39 hits observed at 1 μM), we sought to further extend our kinome analysis of this compound. Evaluating **15** in the DiscoverRx Kinomescan panel (Fig. 4) at 1 μM resulted in a selectivity score of S(35) = 0.008 (number of non-mutant kinases with % control < 35/number of non-mutant kinases tested where positive control = 0% and DMSO = 100%). This was the result of inhibiting, in addition to LRRK2 (18% of control), Tyk2 (19% of control) and JAK3 (29% of control) for a total of 3 out of 392 unique kinases.

We continued to profile **15** and, in particular, were very interested in its brain availability (BA). The in vitro permeability and *P*-gp ER data were predictive of good BA (Table 1). Figure 5 shows the free brain and plasma drug concentrations vs. time plot from which the rat BA for **15**, dosed at 10 mg/kg, was determined.[15] The plot illustrates the instantaneous equilibration between brain and plasma at each time point. The $AUC_{(0\text{-}Tlast)}$-based $K_{p,uu}$ of 0.14 indicated there was 7× brain impairment (BI) in the rat. This

Table 4
Core variation on [1,2,4]triazolo[4,3-*b*]pyridazine

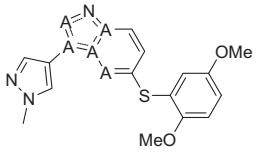

Compd	Core	LRRK2 IC_{50}[a] (nM)	LE/LipE[b]	LRRK2 WC IC_{50}[c] (nM)	HLM[d]	P_{app}[e]	*P*-gp[f]
32	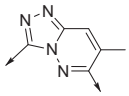	>32,000	0.23/2.12	nt	56	13	2.57
33	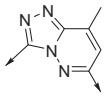	>32,000	0.23/2.12	nt	38	20	1.83
34	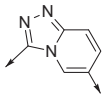	1461	0.31/3.07	nt	57	17	1.56
35	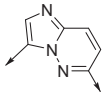	69	0.38/4.31	400	156	12	1.10
36	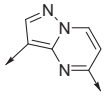	64	0.38/4.18	488	97	10	2.07
37	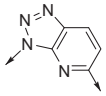	525	0.33/3.13	5240	221	nt	2.39
38	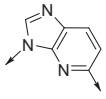	661	0.32/2.84	5850	110	17	1.04
39	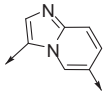	1145	0.31/2.16	nt	206	10	1.51
40	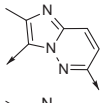	115	0.35/4.12	945	>300	13	1.00
41	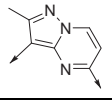	110	0.35/3.98	759	>300	10	1.52

[a] Geometric mean of $n \geqslant 2$ for wild-type LRRK2 at 1 mM ATP.
[b] Calculated from 1 mM ATP IC_{50} using *c*log*P* values.
[c] Geometric mean of $n \geqslant 2$ for whole cell pS935 determinations in wild-type LRRK2.
[d] Human liver microsomal clearance (mL/min/kg).
[e] Passive permeability (AB $\times 10^{-6}$ cm/s).
[f] MDR1 Efflux Ratio (BA/AB). nt = not tested.

apparent in vitro/in vivo disconnect was further investigated. We had already shown that **15** was not a *P*-gp substrate (Table 1). BCRP (breast cancer related protein) is another transporter expressed at the BBB that could also contribute to this BI. Submitting **15** to our mouse BCRP assay led to the conclusion it was a substrate (Table 5). Interestingly, the BA found for **15** stands in contrast to the BA found for **35** ($K_{pu,u}$ = 0.42) or **36** ($K_{pu,u}$ = 0.27) and could be potentially rationalized by the observation they were neither a *P*-gp or BCRP substrates. It is unclear whether this rat BI would translate to humans as it is known that the level of transporter expression at the BBB is species dependent.[16]

Although brain impaired, we felt the excellent kinase selectivity profile of **15** would prove useful for probing the peripheral safety liabilities of LRRK2 kinase inhibition as LRRK2 KO animals have revealed kidney and lung phenotypes.[17] We decided to conduct a PK/PD study with **15** where it was orally dosed in mice at 0, 30, and 300 mg/kg/day for 14 days (5 males/dose). Endpoints included a full hematologic and clinical chemistry profile on day 14 along with a macroscopic examination at necropsy and a microscopic examination of selected tissues (kidney, liver, heart, lung, spleen, and thymus). Table 6 summarizes the data generated from that study indicating the exposures achieved and the findings observed. The result supported the highly selective nature of this compound, in that no treatment related findings were observed at high exposures.

We were disappointed to learn of the results from an in vivo determination of the pS935 endpoint[18] in brain and kidney. As one might expect for a compound that is brain impaired, **15**

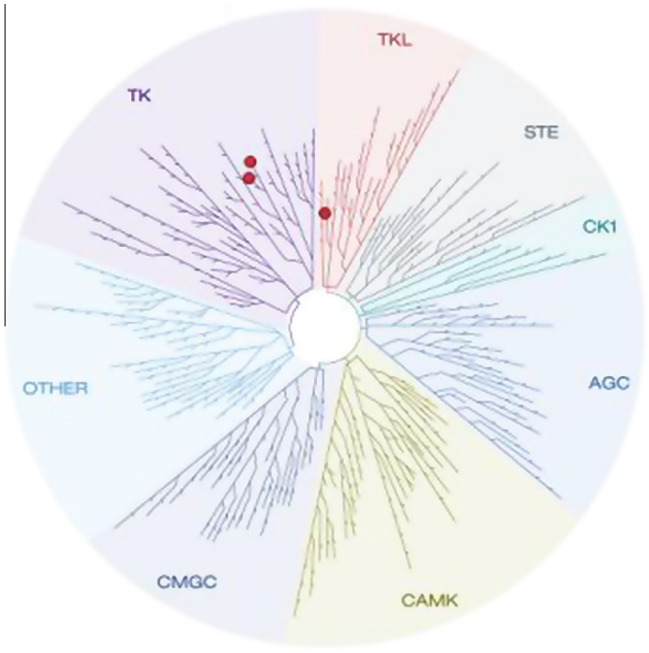

Figure 4. TREEspot™ visualization of kinome selectivity for **15** at 1 μM.

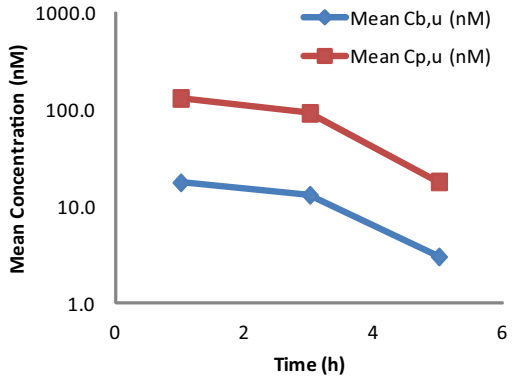

Figure 5. Plot of rat free brain and plasma vs time for **15**.

Table 6
Safety findings from a multi-dose, 14 day mouse study

Dose (mg/kg)	C_{max} (ng/mL)	$AUC_{(0-24)}$ (ng h/mL)	Findings
0	–	–	No treatment-related findings
30	200	350	No treatment-related findings
300	12,870	20,900	No treatment-related findings

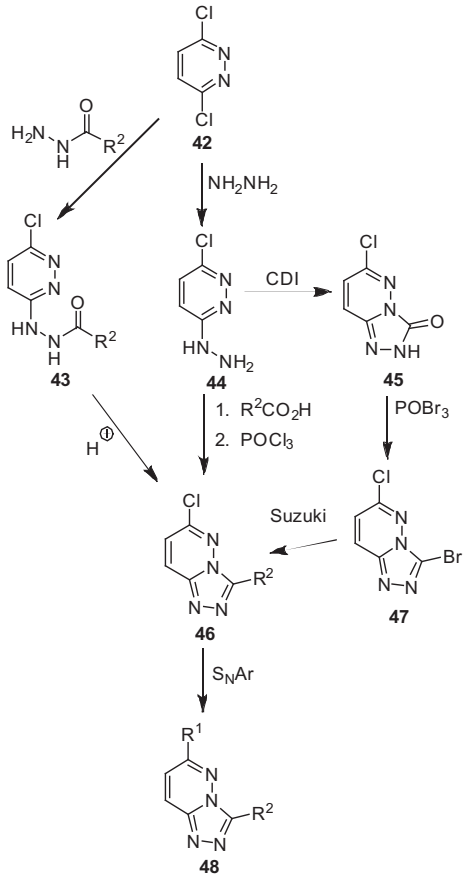

Scheme 1. Synthetic route for preparing the triazolopyridazines.

behaved similar to LRRK2-IN-1,[8a] in that no effect on the pS935 levels was found even after 14 days at 300 mg/kg/day. More surprising was a similar observation for the kidney. Despite the highly perfused nature of the kidney and the determination that **15** exhibited a $C_{kidney}/C_{plasma} \sim 2$, no change in pS935 levels were observed at any dose.

Synthetically, triazolopyridazines **48** could be prepared in a straightforward manner from commercially available **42**.[8i,21] Scheme 1 outlines routes for this conversion. Exposure of **42** to hydrazine afforded **44** which could be converted in 2 steps to **46** by amide formation followed by ring closure. Alternatively, the overall conversion of **42** to **46** could be conducted by displacement of the chloride with the hydrazoic acid followed by ring closure via **43**. To potentially enable library protocols, dihalide **47** could be prepared from **44** by ring closure and treatment of the resulting triazinone **45** with $POBr_3$. Using the appropriate nucleophiles resulted in the conversion of **46** to **48**. The generation of **48** from **47** could be achieved by sequential Suzuki cross-coupling and S_NAr reaction through the intermediary **46**.

Table 5
Mouse BCRP[a] data for selected compounds

Compd	Induced (Dox) [b]			Non-induced			Ratio of ratios[c]
	AB ($\times 10^{-6}$)	BA ($\times 10^{-6}$)	ER	AB ($\times 10^{-6}$)	BA ($\times 10^{-6}$)	ER	
15	10	39	3.9	33	28	0.9	4.5
35	25	28	1.1	24	24	1	1.1
36	29	27	0.9	29	25	0.9	1.1

[a] BCRP transfected cells ($n = 3$) using prazosin as positive control and quinidine as negative control.
[b] BCRP induced with doxycycline.
[c] Substrate defined as having a ratio of ratios significantly higher than 1, calculated by ER(induced)/ER(non-induced).

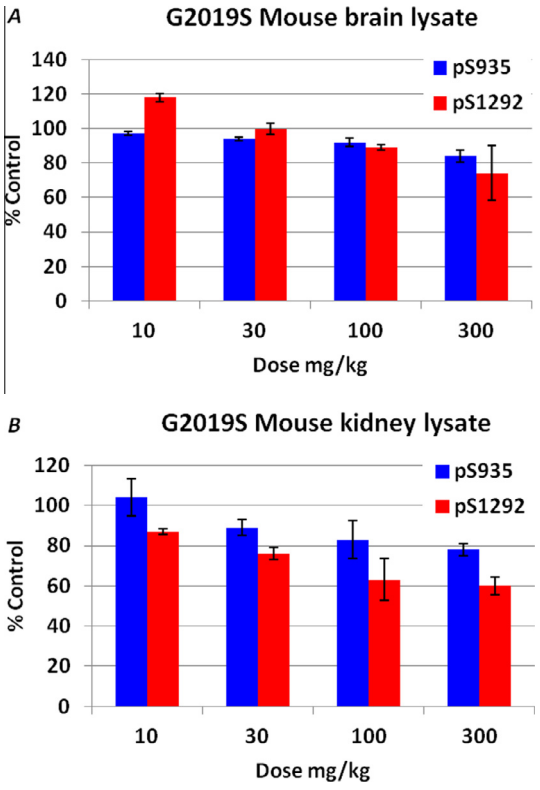

Figure 6. [19]Dose response of **15** in G2019S transgenic mice showing pS935 and pS1292 readouts for brain (A) and kidney (B) at 90 min (mean ± SEM is shown, each endpoints based on data from three transgenic mice).

Modest changes in key PD endpoints, measured at 90 min, could be observed when **15** was dosed in G2019S transgenic mice (Fig. 6).[19] Dosing **15** up to 300 mg/kg achieved an unbound brain concentration of 1809 nM and exhibited about a 20% decrease in the phosphorylation of the S935 and S1292[20] residues (Fig. 6A). Kidney showed a decrease in phosphorylation of ~20% for S935 and ~40% for S1292 (Fig. 6B).

In summary, an HTS campaign identified triazolopyridazines as having potency at LRRK2. This scaffold was subjected to SAR optimization to not only improve target potency but to also maintain good predicted brain availability using passive permeability and *P*-gp efflux as leading indicators. Surrogate crystallography enabled the identification of a binding pose that was consistent with the observed SAR. We identified **15** as a tool compound exhibiting a good in vitro/cellular profile. While it was not a *P*-gp substrate, it was found to be a substrate for BCRP which appears to have limited its in vivo effectiveness. Our focus has now shifted to the other HTS hits and we will disclose those data in due course.

Acknowledgments

We thank John Knafels for crystal soaking and freezing experiments.

References and notes

1. (a) Jellinger, K. A. *Mov. Disord.* **2012**, *27*, 8; (b) Poulopoulos, M.; Levy, O. A.; Alcalay, R. N. *Mov. Disord.* **2012**, *27*, 831.
2. (a) Satake, W.; Nabalyashi, Y.; Mizuta, I.; Hirota, Y.; Ito, C.; Kubo, M.; Kawaguchi, T.; Tsunoda, T.; Watanabe, M.; Takeda, A.; Tomiyama, H.; Nakashima, K.; Hasegawa, K.; Obata, F.; Yoshikwa, T.; Kawakami, H.; Sakoda, S.; Yamamoto, M.; Hattori, N.; Murata, M.; Nakamura, Y.; Toda, T. *Nat. Genet.* **2009**, *41*, 1303; (b) Chang, X.-L.; Mao, X.-Y.; Li, H.-H.; Zhang, J.-H.; Li, N.-N.; Burgunder, J.-M.; Peng, R.; Tan, E.-K. *Am. J. Med. Genet. Part B* **2011**, *156*, 334; (c) Do, C. B.; Tung, J. Y.; Dorfman, E.; Kiefer, A. K.; Drabant, E. M.; Francke, U.; Mountain, J. L.; Goldman, S. M.; Tanner, C. M.; Langston, J. W.; Wojcicki, A.; Eriksson, N. *PLoS Genet.* **2011**, *7*, e1002141.
3. Anand, V. S.; Braithwaite, S. P. *FEBS J.* **2009**, *276*, 6428.
4. (a) Tsika, E.; Moore, D. J. *Curr. Neurol. Neurosci. Rep.* **2012**, *12*, 251; (b) Kramer, T.; LoMonte, F.; Goering, S.; Amombo, O.; Marlyse, G.; Schmidt, B. *ACS Chem. Neurosci.* **2012**, *3*, 151.
5. (a) Smith, W. W.; Pei, Z.; Jiang, H.; Dawson, V. L.; Dawson, T. M.; Ross, C. A. *Nat. Neurosci.* **2006**, *9*, 1231; (b) Covy, J. P.; Giasson, B. I. *Biochem. Biophys. Res. Commun.* **2009**, *378*, 473; (c) Nichols, R. J.; Dzamko, N.; Hutti, J. E.; Cantley, L. C.; Deak, M.; Moran, J.; Bamborough, P.; Reith, A. D.; Alessi, D. R. *Biochem. J.* **2009**, *424*, 47; (d) Gilsbach, B. K.; Ho, F. Y.; Vetter, I. R.; van Haastert, P. J. M.; Wittinghofer, A.; Kortholt, A. *PNAS* **2012**, *109*, 10322.
6. (a) Sen, S.; Webber, P. J.; West, A. B. *J. Biol. Chem.* **2009**, *284*, 36346; (b) Berger, Z.; Smith, K. A.; LaVoie, M. *J. Biochem.* **2010**, *49*, 5523; (c) Devine, M. J.; Kaganovich, A.; Ryten, M.; Mamais, A.; Trabzuni, D.; Manzoni, C.; McGoldrick, P.; Chan, D.; Dillman, A.; Zerle, J.; Horan, S.; Taanman, J.-W.; Hardy, J.; Marti-Masso, J.-F.; Healey, D.; Schapira, A. H.; Wolozin, B.; Bandopadhyay, R.; Cookson, M. R.; van der Brug, M. P.; Lewis, P. A. *PLoS One* **2011**, *6*, e22489; (d) Taymans, J.-M.; Vancraenenbroeck, R.; Ollikainen, P.; Beilina, A.; Lobbestael, E.; De Maeyer, M.; Baekelandt, V.; Cookson, M. R. *PLoS One* **2011**, *6*, e23207.
7. Lee, B. D.; Shin, J.-H.; VanKampen, J.; Petucelli, L.; West, A. B.; Ko, H. S.; Lee, Y.-I.; Maguire-Zeiss, K. A.; Bowers, W. J.; Federoff, H. J.; Dawson, V. L.; Dawson, T. M. *Nat. Med.* **2010**, *16*, 998.
8. (a) Deng, X.; Dzamko, N.; Prescott, A.; Davies, P.; Liu, Q.; Yang, Q.; Lee, J.-D.; Patricelli, M. P.; Nomanbhoy, T. K.; Alessi, D. R.; Gray, N. S. *Nat. Chem. Biol.* **2011**, *7*, 203; (b) Ramsden, N.; Perrin, J.; Ren, Z.; Lee, B. D.; Zinn, N.; Dawson, V. L.; Tam, D.; Bova, M.; Lang, M.; Drewes, G.; Bantscheff, M.; Bard, F.; Dawson, T. M.; Hopf, C. *ACS Chem. Biol.* **2011**, *6*, 1021; (c) Zhang, J.; Deng, X.; Choi, H. G.; Alessi, D. R.; Gray, N. S. *Bioorg. Med. Chem. Lett.* **2012**, *22*, 1864; (d) Reith, A. D.; Bamborough, P.; Jandu, K.; Andreotti, D.; Mensah, L.; Dossang, P.; Choi, H. G.; Deng, X.; Zhang, J.; Alessi, D. R.; Gray, N. S. *Bioorg. Med. Chem. Lett.* **2012**, *22*, 5625; (e) Chen, H.; Chan, B. K.; Drummond, J.; Estrada, A. A.; Gunzner-Toste, J.; Liu, X.; Liu, Y.; Moffat, J.; Shore, D.; Sweeney, Z. K.; Tran, T.; Wang, S.; Zhao, G.; Zhu, H.; Burdick, D. J. *J. Med. Chem.* **2012**, *55*, 5536; (f) Estrada, A. A.; Liu, X.; Baker-Glenn, C.; Beresford, A.; Burdick, D. J.; Chambers, M.; Chan, B. K.; Chen, H.; Ding, X.; DiPasquale, A. G.; Dominguez, S. L.; Dotson, J.; Drummond, J.; Flagella, M.; Flynn, S.; Fuji, R.; Gill, A.; Gunzner-Toste, J.; Harris, S. F.; Heffron, T. P.; Kleinheinz, T.; Lee, D. W.; Le Pichon, C. E.; Lyssikatos, J. P.; Medhurst, A. D.; Moffat, J. G.; Mukund, S.; Nash, K.; Scearce-Levie, K.; Sheng, Z.; Shore, D. G.; Tran, T.; Trivedi, N.; Wang, S.; Zhang, S.; Zhang, X.; Zhao, G.; Zhu, H.; Sweeney, Z. K. *J. Med. Chem.* **2012**, *55*, 9416; (g) Garofalo, A. W.; Adler, M.; Aubele, D. L.; Brigham, E. F.; Chian, D.; Franzini, M.; Goldbach, E.; Kwong, G. T.; Motter, R.; Probst, G. D.; Quinn, K. P.; Ruslim, L.; Sham, H. L.; Tam, D.; Tanaka, P.; Truong, A. P.; Ye, X. M.; Ren, Z. *Bioorg. Med. Chem. Lett.* **2013**, *23*, 1974; (h) Chan, B. K.; Estrada, A. A.; Chen, H.; Atherall, J.; Baker-Glenn, C.; Beresford, A.; Burdick, D. J.; Chambers, M.; Dominguez, S. L.; Drummond, J.; Gill, A.; Kleinheinz, T.; Le Pichon, C. E.; Medhurst, A. D.; Liu, X.; Moffat, J. G.; Nash, K.; Scearce-Levie, K.; Sheng, Z.; Shore, D. G.; Van de Poel, H.; Zhang, S.; Zhu, H.; Sweeney, Z. K. *ACS Med. Chem. Lett.* **2013**, *4*, 85; (i) Franzini, M.; Ye, X. M.; Adler, M.; Aubele, D. L.; Garofalo, A. W.; Gauby, S.; Goldbach, E.; Probst, G. D.; Quinn, K. P.; Santiago, P.; Sham, H. L.; Tam, D.; Truong, A.; Ren, Z. *Bioorg. Med. Chem. Lett.* **2013**, *23*, 1967; (j) Estrada, A. A.; Chan, B. K.; Baker-Glenn, C.; Beresford, A.; Burdick, D. J.; Chambers, M.; Chen, H.; Dominguez, S. L.; Dotson, J.; Drummond, J.; Flagella, M.; Fuji, R.; Gill, A.; Halladay, J.; Harris, S. F.; Heffron, T. P.; Kleinheinz, T.; Lee, D. W.; Pichon, C. E. L.; Liu, X.; Lyssikatos, J. P.; Medhurst, A. D.; Moffat, J. G.; Nash, K.; Scearce-Levie, K.; Sheng, Z.; Shore, D. G.; Wong, S.; Zhang, S.; Zhang, X.; Zhu, H.; Sweeney, Z. K. *J. Med. Chem.* **2014**, *57*, 921.
9. Luerman, G. C.; Nguyen, C.; Samaroo, H.; Loos, P.; Xi, H.; Hurtado-Lorenzo, A.; Needle, E.; Noell, G. S.; Galatsis, P.; Dunlop, J.; Geoghegan, K. F.; Hirst, W. D. *J. Neurochem.* **2014**, *128*, 561.
10. LRRK2 kinase activity was measured using LANTHA Screen technology from Invitrogen. GST-tagged truncated LRRK2 from Invitrogen (Cat # PV4874) or mutant G2019S LRRK2 (Invitrogen cat # PV4881) was incubated with fluorescein-labeled peptide substrate LRRKtide (Invitrogen cat # PR8976A), in the presence of a dose response of compound. Upon completion, the assay was stopped and detected with a terbium labeled anti-phospho-ERM antibody (Invitrogen, cat # PR8975A). The assay was carried out under the following protocol: 3 μL of a working solution of substrate (233 nM LRRKtide, 117 μM ATP) prepared in assay buffer (50 mM HEEPES, pH 7.5, 3 mM $MgCl_2$, with 2 mM DTT and 0.01% Brij35 added fresh) was added to a low volume Greiner 384-well plate. The compound dose response was prepared by diluting compound to a top concentration of 3.16 mM in 100% DMSO and serial diluted by half-log in DMSO 11 times. Aliquots (3.5 μL) of the 100% DMSO dose response were mixed with 46.5 μL water then 1 μL of this mixture was added to the 3 μL substrate mix in the 384-well plate. The kinase reaction was started with 3 μL of a working solution of LRRK2 enzyme at a concentration of 4 μg/mL. The final reaction concentrations were 100 nM LRRKtide, 50 μM ATP, 1.7 μg/mL LRRK2 enzyme and a compound dose response with a top dose of 32 μM. The reaction was allowed to progress at room temperature for two hours or 90 minutes for the mutant protein and then stopped with the addition of 7 μL of detection buffer (20 mM Tris pH 7.6, 0.01% NP-40, 0.02% NaN_3, 6 mM EDTA with 2 nM terbium labeled anti-phospho-ERM). After an incubation of 1 h at room temperature, the plate was read on an Envision with an excitation wavelength of 340 nm and a reading emission at both 520 nm and 495 nm. The ratio of the 520 nm and 495 nm emission was used to analyze the data. *LRRK2 whole cell assay method:*

Transfection and cell treatment—HEK 293 cells were transiently transfected with full length LRRK2 using a DNA:Lipofectamine 2000 ratio of 1:2.5 (μg:μL) in a 85–90% confluent T175 flask. After 6 hours the transfection media was replaced with growth media (DMEM+10%FBS) and incubated overnight. The following day cells were harvested and plated into clear tissue culture treated 384-well plates at 10,000 cells/well and allowed to incubate overnight. The next day cells were treated with a dose response of compound for 90 min at 37 °C, 5% CO_2. After compound treatment, cells were lysed with 15 μL lysis buffer (Lantha Lysis buffer (Invitrogen, PV5598) with protease inhibitor (Sigma P2714), 0.1% SDS, 1 mM Na_3PO_4, 17.5 mM $Na_2H_2P_2O_7$, 25 mM NaF, 1 mM PMSF) for 30 minutes at 4 °C and frozen at −80 °C for 30 min to ensure complete lysis. 8 μL of the lysed cells was then transferred to ELISA plates coated with LRRK2 capture antibody and blocked with BSA and allowed to incubate overnight at 4 °C. ELISA—384-well high binding plates (Greiner 781074) were coated with 10 μL of mouse monoclonal anti-LRRK2 antibody (Covance SIG-39840) at a final concentration of 10 μg/mL in sodium bicarbonate buffer at pH 9.5 and incubated overnight at 4 °C. Plates were then blocked with 1% BSA in PBS-Tween (0.05%) for 1 hour and washed in PBS-Tween before receiving 8 μL of treated cell lysis. The next day plates were washed and incubated with anti-LRRK2 phospho-S935 antibody (Abcam, UDD210(12)) at 1:2000 in PBS-Tween for 1 hour then washed and incubated with an anti-Rabbit-HRP antibody (GE Healthcare NA9340V) for 1 hour. Plates were washed one final time and signal was detected with SuperSignal ELISA Pico Chemiluminescent Substrate (Pierce 37069).

11. (a) Meanwell, N. A. *Chem. Res. Toxicol.* **2011**, *24*, 1420; (b) Edwards, M. P.; Price, D. A. *Ann. Rep. Med. Chem.* **2010**, *45*, 381; (c) Wager, T. T.; Hou, X.; Verhoest, P. R.; Villalobos, A. *ACS Chem. Neurosci.* **2010**, *1*, 435.
12. Kinome selectivity screening (KSS) against a panel of 39 kinases, chosen to broadly cover the kinome
13. Groom, C. R.; Allen, F. H.; Henderson, S. The Cambridge Structural Database (CSD). In: Reference Module in Chemistry, Molecular Sciences and Chemical Engineering, Elsevier, Waltham, MA, USA, **2013**.
14. Bruno, I. J.; Cole, J. C.; Kessler, M.; Luo, J.; Motherwell, W. D. S.; Purkis, L. H.; Smith, B. R.; Taylor, R.; Cooper, R. I.; Harris, S. E.; Orpen, A. G. *J. Chem. Inf. Comput. Sci.* **2004**, *44*, 2133.
15. For a review of blood brain barrier penetration see: Reichel, A. *Chem. Biodiversity* **2009**, *6*, 2030.
16. (a) Uchida, Y.; Ohtsuki, S.; Katsukura, Y.; Ikeda, C.; Suzuki, T.; Kamiie, J.; Terasaki, T. *J. Neurochem.* **2011**, *117*, 333; (b) Ito, K.; Uchida, Y.; Ohtsuki, S.; Aizawa, S.; Kawakami, H.; Katukura, Y.; Kamiie, J.; Terasaki, T. *J. Pharma. Sci.* **2011**, *100*, 3939.
17. (a) Miklavc, P.; Ehinger, K.; Thompson, K. E.; Hobi, N.; Shimshek, D. R.; Frick, M. *PLoS One* **2014**, *9*, e84926; (b) Ness, D.; Ren, Z.; Gardi, S.; Sharpnack, D.; Johnson, V. J.; Brennan, R. J.; Brigham, E. F.; Olaharski, A. J. *PLoS One* **2013**, *8*, e66164; (c) Herzig, M. C.; Kolly, C.; Persohn, E.; Theil, D.; Schweizer, T.; Hafner, T.; Stemmelen, C.; Troxler, T. J.; Schmid, P.; Danner, S.; Schnell, C. R.; Mueller, M.; Kinzel, B.; Grevot, A.; Bolognani, F.; Stirn, M.; Kuhn, R. R.; Kaupmann, K.; ver der Putten, P. H.; Rovelli, G.; Shimshek, D. R. *Hum. Mol. Genet.* **2011**, *20*, 4209.
18. Dzamko, N.; Deak, M.; Hentati, F.; Reith, A. D.; Prescott, A. R.; Alessi, D. R.; Nichols, R. J. *Biochem. J.* **2010**, *430*, 405.
19. Custom generated antibody against pS1292 LRRK2 was used. Specificity against pS1292 was verified using pS1292A. Brains and kidneys were homogenized in lysis buffer (50 mM Tris-HCl pH 7.5, 150 mM NaCl, 1% Triton-X100, 5% Glycerol, 10 mM PPA, 20 mM NaF, 2 mM Na_3VO_4, 2 mM EGTA, 2 mM EDTA), incubated on ice for 30 min and centrifuged at 4° C for 10 min at 20,800 g. Supernatant was used for western blot analysis. Vehicle (1 Meq of 1 N HCl, 10% NMP (1-methyl-2-pyrrolidone) in 20% SBECD (beta-cyclodextrin sulfobutyl ether) solution) was used as a control.
20. Sheng, Z.; Zhang, S.; Bustos, D.; Kleinheinz, T.; Le Pichon, C. E.; Dominguez, S. L.; Solanoy, H. O.; Drummond, J.; Zhang, X.; Ding, X.; Cai, F.; Song, Q.; Li, X.; Yue, Z.; van der Brug, M. P.; Durdick, D. J.; Gunzner-Toste, J.; Chen, H.; Liu, X.; Estrada, A. A.; Sweeney, Z. K.; Scearce-Levie, K.; Moffat, J. G.; Kirkpatrick, D. S.; Zhu, H. *Sci. Transl. Med.* **2012**, *4*(164r), a161.
21. (a) Collins, I.; Castro, J. L.; Street, L. J. *Tetrahedron Lett.* **2000**, *41*, 781; (b) Street, L. J.; Sternfeld, F.; Jelley, R. A.; Reeve, A. J.; Carling, R. W.; Moore, K. W.; McKernan, R. M.; Sohal, B.; Cook, S.; Pike, A.; Dawson, G. R.; Bromidge, F. A.; Wafford, K. A.; Seabrook, G. R.; Thompson, S. A.; Marshall, G.; Pillai, G. V.; Castron, J. L.; Atack, J. R.; MacLeod, A. M. *J. Med. Chem.* **2004**, *47*, 3642; (c) Thiel, O. R.; Achmatowicz, M. M.; Reichelt, A.; Larsen, R. D. *Angew. Chem., Int. Ed.* **2010**, *49*, 8395; (d) Heinelt, U.; Wehner, V.; Herrmann, M.; Schoenafinger, K.; Steinhagen, H.; Scheiper, B. Patent Application 2009097970. **2009**.; (e) Aldrich, L. N.; Lebois, E. P.; Lewis, L. M.; Nalywajko, N. T.; Niswender, C. M.; Weaver, C. D.; Conn, P. J.; Lindsley, C. W. *Tetrahedron Lett.* **2009**, *50*, 212.